Magnier, Benjamin; Claude, Nicolas; Villaret, Catherine; Rodrigues, Stéphane; Tassi, Pablo

Numerical Simulation of Flow Structures in the Presence of Alternate and Transverse Bars: Application to the Loire River (France)

TUC 2013, 16-18/10/2013, Karlsruhe - Kopmann, Goll (eds.) - © 2013 Bundesanstalt für Wasserbau ISBN 978-3-939230-07-6

Numerical simulation of flow structures in the presence of alternate and transverse bars: application to the Loire river (France)

B. Magnier[1,2], N. Claude[2, 3] , C. Villaret[2] , S. Rodrigues[4] and P. Tassi[2]

[1] Institut de Physique du Globe de Paris
Paris France

[2] EDF R&D - Laboratoire Saint Venant
Chatou, France

[3] Ecole des Nationale des Ponts et Chaussées
Champs sur Marne, France

[4] E.A 6293 GéHCO, Université François Rabelais
Tours, France

Abstract—**In this study, the module TELEMAC-3D is used to analyse the flow behaviour in the presence of alternate and transverse bars. This particular bar organization has been poorly studied in the literature and presents great interest for the planing of dredging operations in rivers like the Loire in France. Three-dimensional numerical results showed that the main flow structure is defined by the channel planform and bars configurations. The roughness-length distance strongly influences the velocity near the bed and the increasing of the mesh resolution impacts the bed resistance mechanisms and, in consequence, the distribution of the velocity profiles.**

I. INTRODUCTION

Bars are ubiquitous morphological macroforms that interact with the flow and sediment transport processes in rivers with important bedload transport rates [2]. Alternate bars, whose structure is characterized by a sequence of steep consecutive diagonal fronts and deep pools at the downstream face, have been extensively investigated both theoretically and through flume studies, e.g. [1, 2, 3, 4]. More complicated macroform patterns, such as transverse, central or multiple configurations can be found in wider reaches, e.g. [5, 6].

Bars can be classified as forced or free. Forced bars arise from a forcing effect that can have an anthropic or natural origin, such as channel curvature, width variations or the presence of confluence/diffluence zones in the channel. Free bars, on the other hand, can arise from an inherent instability of the erodible bottom subject to a turbulent flow [5]. Further details can be found in the companion paper presented in this conference [7].

Depending on the forcing mechanism, bar patterns show different configurations. Forced bars that are associated with a flow in a variable-width channel appear as mid-channel bars or transverse bar, or as two symmetrical lateral bars [8]. The formation of central or transverse bars could be associated to an antisymmetric forcing such as a channel curvature, while alternate bars can appear as a response to instability in the channel bed or by the presence of a repetitive sequence of width variations.

Furthermore, Wu *et al.* [8] pointed out that the presence of free bars in a "forced bar" configuration could give rise to a "mixed" organization (free + forced), arranged in alternate or transversal configurations. Coexisting free and forced bars have been extensively studied in meandering channels. In contrast, the presence of mixed bars in widening/narrowing channels has received little attention [9].

As highlighted by Claude *et al.* [10], the site of Bréhémont in the middle reach of the Loire river in France presents forcing effects caused by channel width variations that induce the presence of alternate and transverse bars over short periods of time, even in a slow hydrodynamic context. To the best of our knowledge, this particular bar organization has been poorly studied in the literature.

In this work, the three-dimensional (3D) hydrodynamic models TELEMAC-3D is calibrated for the site of Bréhémont on the Loire River from a large dataset of high-quality field surveys based on Acoustic Doppler Current Profiler (ADCP) measurements. The validated model is then used to analyze the flow behaviour in the presence of alternate and transverse bars. The plan form and variable bed topography (obtained from multibeam echosoundings) present a complex hydrodynamic behavior in which a number of physical processes are investigated, such as the impact of roughness-length treatment due to "sub-grid" or non-resolved effects of bed roughness [11].

II. SITE AND FIELD MEASUREMENTS

The Loire River, the largest river in France, is 1,020 km long and drains a catchment area of 117,000 km². The study site is located at the village of Bréhémont (47°17'43.31''N, 0°20'33.80''E) in the middle reaches of the Loire River. At the study site, the Loire system presents a multiple-channel pattern. Bed materials are constituted by sands and gravels. The main channel is composed of an expansion zone followed by a contraction area occupied by migrating bars (Fig. 1). These macroforms can adopt successively an alternate or a transverse configuration (Fig. 1) [9]. The channel width varies between 175 and 300 m.

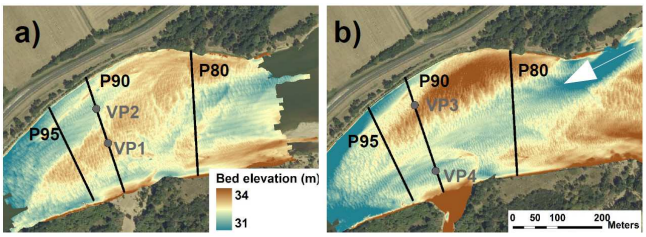

Figure 1. Study site. Black lines: ADCP profiles. Grey points: location vertical velocity profiles. (a) Transverse (22/06/10); (b) alternate (27/12/10) bar configuration. The white arrow indicates the direction of the flow.

Nineteen daily field measurements were performed during the study with a multibeam echosounder and an ADCP. Thus, three floods were monitored with a high temporal resolution: one annual flood in June 2010 (maximal discharge of 1030 m^3/s) and two 2-year floods in December 2010 (maximal discharge of 1950 m^3/s). More details are given in [9].

III. MATHEMATICAL MODEL AND NUMERICAL TOOL

The 3D hydrodynamics field is computed with the 3D hydrodynamics code belonging to the open source TELEMAC-MASCARET system (TMS), TELEMAC-3D. The TMS is currently developed by the R&D department of Electricité de France (EDF) and TELEMAC Consortium members.

TELEMAC-3D solves the 3D Navier-Stokes equations with a finite element discretization under a non-hydrostatic approximation. The code has been fully parallelized using the Message Passing Interface paradigm (MPI). The non-hydrostatic approximation is based on the pressure tained in the first plane above the bottom, with u and v the components of the 3D velocity field, and κ the von Karman's constant (= 0.4). Turbulent stresses and turbulent fluxes are modelled using turbulent viscosity and turbulent gradient diffusion hypothesis, which respectively introduce eddy viscosity and eddy diffusivity. Several turbulence-closure models are available in TELEMAC-3D, see e.g. [12]. In this study, the standard k-ε turbulence model is used.

IV. MODEL CALIBRATION AND 3D NUMERICAL RESULTS

A. Mesh description

The 3D finite element mesh is obtained by first dividing a two-dimensional domain with non-overlapping linear triangles (with a mean size of 10 m) and then by extruding each triangle along the vertical direction into linear prismatic columns that exactly fit the bottom and the free-surface. In doing so, each column can be partitioned into non-overlapping layers, requiring that two adjacent layers comprise the same number of prisms.

B. Model calibration

Model calibration is performed by comparing model predictions with averaged ADCP velocity measurements of streamwise velocities and velocity profiles at different cross-sections surveys, see Fig. 1. The optimization of model prediction is done by using a roughness-length representation based on the Nikuradse coefficient k_s. The decomposition into hydrostatic and hydrodynamic parts, allowing an accurate computation of the vertical velocity, which is coupled to the whole system of equations.

In the present study, boundary conditions are specified as follows: at the domain inflow all flow components are prescribed by imposing a velocity profile to provide a certain inflow discharge. At the domain outlet the normal gradients of all variables are set equal to zero. On the solid boundaries the velocities tangential and normal to the boundary are set to zero. Inflow and outflow boundary conditions used for the different models and configurations are shown in Table I.

The parameterization of bed shear stress is done by assuming the validity of the « law of the wall », which applies on a relatively thin layer near the bed (z/h < 0.20, with h the mean flow depth) [11]. In TELEMAC-3D, this approximation is used to determine the shear velocity u_* (subroutine `tfond.f`) at a distance equal to the altitude of the first plane above the bottom z':

$$u_* = \frac{\kappa |u|_r}{\ln(z'/z_0)} \quad (1)$$

where z_0 is a characteristic length scale. For hydraulically rough flows, which is the situation commonly found in natural channels $z_0 = k_s/30$, with k_s the Nikuradse's effective roughness-length. In (1), $|u|_r = (u^2 + v^2)^{1/2}$ is the magnitude of the velocity con

friction coefficients used in the models are presented in Table I.

TABLE I. BOUNDARY CONDITIONS AND BED ROUGHNESS COEFFICIENTS USED IN THE MODELS

Mesh	Flow rates (m^3/s)	Downstream water surface elevation (m)	Roughness coefficient (m)
Transverse Bar	400	34.38	0.07
	700	35.19	0.12
	1000	35.77	0.3
Alternate Bars	700	35.21	0.275
	1000	35.91	0.125
	2000	37.39	0.0975

In general, streamwise velocities are well represented by the model for the different flow discharges (Fig. 2a and 2c). Concerning the velocity profiles, for the transverse bar configuration, comparisons between measurements and numerical results are done on P90 (Fig. 1a) on VP1 (over the bar) and VP2 (thalweg). For the alternate bars configuration, comparisons are performed on P90 (Fig. 1b) on VP3 (over the right bar) and VP4 (thalweg). For both configurations,

the numerical results are in agreement with field measurements (Fig.3a and 3c), except at low discharge (400 m³/s) for the transverse bar configuration and high discharge (2000 m³/s) for the alternate bar configuration (Fig. 3b and 3d).

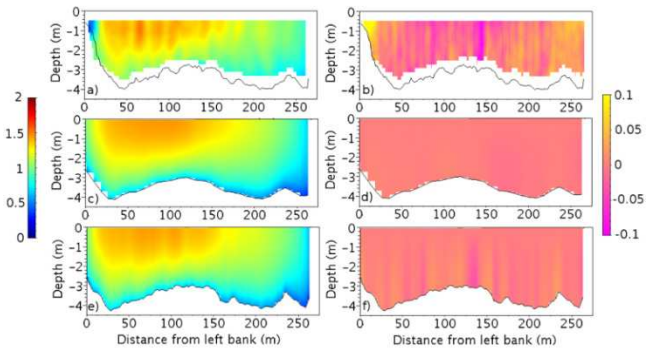

Figure 2. Cross-sectional and vertical distribution of velocities (m/s) and vertical velocities (m/s) on P90 with a transverse bar configuration for 1000 m³/s and *ks*= 0.3 m; a) measured velocities, b) measured vertical velocities, c) velocities predicted by the model with the basic mesh (element size of approx. 10 m), d) vertical velocities predicted by the model with the basic mesh, e) velocities predicted by the model with the refined and re-interpolated mesh (element size of approx. 2.5 m), f) vertical velocities predicted by the model with the refined and re-interpolated mesh. Positive vertical velocities are for upwelling, negative vertical velocities are for down welling.

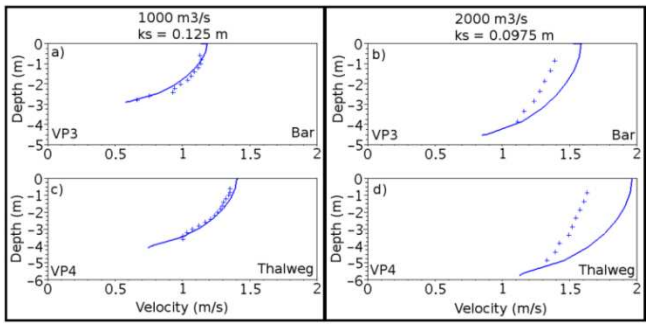

Figure 3. Measured (+) and predicted (solid lines) vertical velocity profiles for the alternate bar configuration, a) over the bar at 1000 m³/s, b) over the bar at 2000 m³/s, c) over the thalweg 1000 m³/s, d) over the thalweg 2000 m³/s.

C. 3D numerical results

1) Influence of the roughness-length

Fig. 4 presents a comparison between measurements and numerical results of velocity profiles for different values of k_s. These plots show that the shape of the vertical velocity profiles depends on the roughness coefficient. This parameter strongly influences the velocity near the bed and through a significant portion of the water column, while its impact on the velocity close to the surface decreases with a deeper depth. As expected, the effect of decreasing the Nikuradse's roughness-length values will produce larger velocity gradients near the bottom. Furthermore, for the same water discharge, the *ks* do not have the same influence on the velocity profile in pools and on bars (Fig. 4a and 4b).

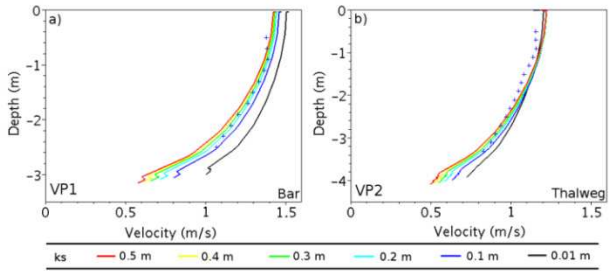

Figure 4. Vertical velocity profiles for different roughness coefficients for the transverse bar configuration at 1000 m³/s; a) over the bar, b) in the pool close to the right bank. Field data are indicated with +.

2) Influence of the mesh resolution and convergence of the model

The convergence of the model and mesh dependency is studied by analyzing the distribution of the velocity profiles. Fig. 5 presents the velocity profile predictions obtained with a mesh size of approx. 10 m and a mesh refined by a factor of 16 in the horizontal plane, resulting in a mesh size of approx. 2.5 m in the study zone. For this case, the finer mesh has not been re-interpolated. The results show that the velocity profiles remain almost unaffected to the mesh refinement. For a horizontal mesh discretization with a mesh size of approx. 10 m, the convergence of the model to the refinement in the vertical direction show little impact on the model results (Fig. 5). Further analysis showed that, in our study, a distribution of eight vertical planes is an optimal compromise between model efficiency and accuracy.

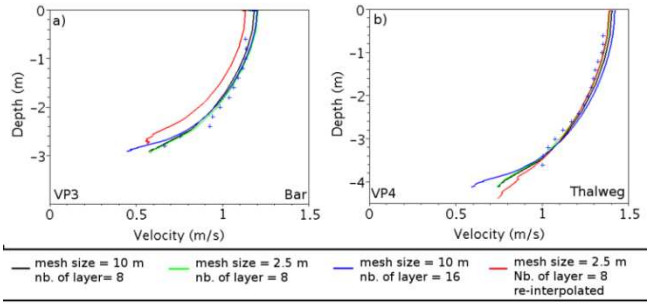

Figure 5. Influence of mesh refinement and reinterpolation on vertical velocity profiles at 1000 m³/s in alternate bar configuration. a) over the bar, b) over the thalweg. Field data are indicated with +.

Re-interpolating the topographic information into the nodes of a spatially refined mesh can lead to significant changes in the model results, as is shown in Fig. 2e, 2f and 5. Generally, the refinement and re-interpolation of the meshes do not improve significantly the magnitude of the velocities and the vertical velocities (Fig. 5b). Also, refinement and re-interpolation can give worse predictions (Fig. 5a). However, the horizontal resolution of a mesh size of approx. 2.5 m incorporates small scale topographic features that cannot be captured with a horizontal mesh resolution of 10 m (Fig. 2e and 2f). Therefore, the increase in mesh resolution impacts the bed resistance mechanisms and, in consequence, the distribution of the velocity profiles. Moreover, vertical accuracy can be further improved with the increasing of grid resolution and re-interpolating topographic information. Fig. 2a-f shows a comparison of measured ADCP vertical

velocities and model results for a horizontal mesh resolution of 10 m and a mesh reduced by a factor of 4, respectively. These results show how the mesh resolution affects dramatically the velocity distribution. In this case, the coarse mesh "filters" topographic features that are well captured by the high resolution mesh, with important consequences on the prediction of energy losses and therefore, on the correct evaluation of the shear stresses.

3) Analysis of the flow structure for the transverse and alternate bars configurations

For the transverse and alternate configurations, the streamwise and crosswise velocities are presented respectively in Fig. 6 and 7 for a discharge of 1000 m^3/s. Numerical simulations show that the flow structure and distribution remains almost identical for both the alternate and transverse bars configuration, with higher speeds located in the thalweg, between the left bank and the top of the bars (Fig. 6a and 6b). However, small differences exist between both configurations, as the transverse bar concentrates the flows more to the left part of the channel, leading to higher velocities.

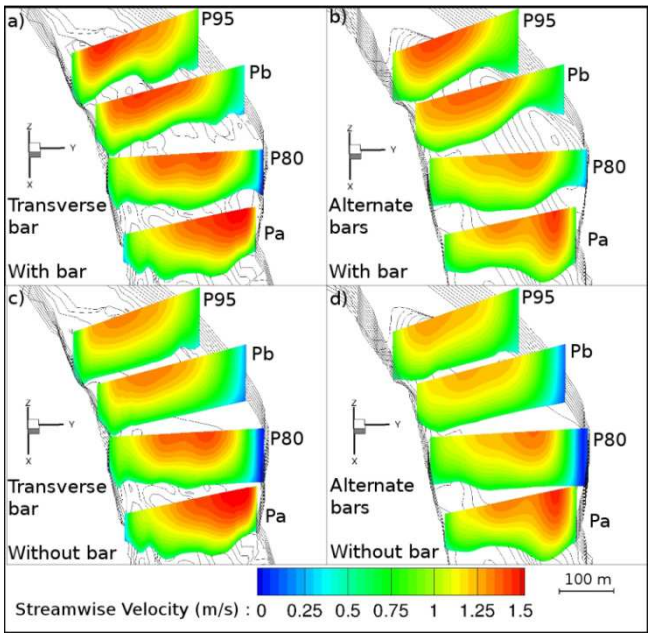

Figure 6. Cross-sectional and vertical distribution of streamwise velocities at 1000 m³/s; a) transverse bar configuration, b) alternate bars configuration, c) transverse bar configuration with the bar deleted, d) alternate bars configuration with the bars deleted.

The analysis of the crosswise velocities shows a flow divergence zone near the left edge of the bars and convergence zones coincident with the position of the right edge of the bars (Fig. 7a and 7b). Flow convergence is also found in the thalweg. The projection of the flow field onto the crosswise section shows a clear difference between the magnitude of the transversal velocity component in the deeper depth zone of the channel with respect of the portion occupied by the bars (see P80 and P95).

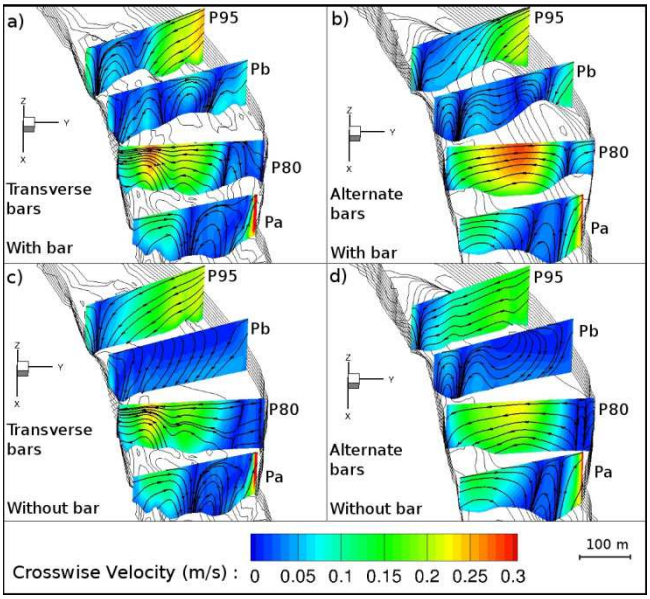

Figure 7. Cross-sectional and vertical distribution of crosswise at 1000 m³/s; a) transverse bar configuration, b) alternate bars configuration, c) transverse bar configuration with the bar deleted, d) alternate bars configuration with the bars deleted. Arrows represent the direction of the crosswise velocities.

To study the influence of the bars on the streamwise and crosswise velocities, two new models were built. These models present similar characteristics than the models presented previously, except that the macroforms were removed from the topographic information. Simulation results are presented in Fig. 6c, 6d, 7c and 7d for a discharge of 1000 m^3/s. Fig. 6 shows that the absence of the bars causes a decreasing of the intensity of the streamwise velocity. Nevertheless, the zones of higher velocities remain almost identical when comparing with those of the topography with the bars.

The effect of the absence of bars seems to be more important for the distribution of the crosswise velocities (Fig. 7). For the profile P80, the absence of the macroforms motorizes a projection of the flow towards the divergence zone near the right bank. On the left bank, crosswise velocities present a lower intensity. At the Pb profile (between profiles P80 and P95), the zones of convergence and divergence of the flow over the bars disappear. Finally, at the profile P95 the transversal velocities exhibit higher velocities than in the presence of bars, while the velocities direction remains almost identical.

V. DISCUSSION AND CONCLUSIONS

Our numerical results showed that the predicted velocities evolve differently according to the water depth when the roughness coefficient is changed (Fig. 4). These observations, similar as those of Sandbach *et al.* [11], show that the influence of the roughness coefficient on the hydrodynamic differs for the different morphological units (bars, thalweg, pool, etc…). This means that during floods (when the values of *ks* change significantly), the the hydrodynamic and the sediment dynamics associated with the bars and the thalweg could follow different evolutions,

and, like for the hydraulic reversal theory (velocity shear stress), could affect the formation of pools and riffles [13].

Furthermore, for a water discharge and a bar configuration, the vertical velocity profiles obtained from the models are in relative agreement with the field measurements according to their location (thalweg or bar) (Fig. 3a, 3c and 5). These results may indicate a spatial variability of the bed roughness. Thus, the bars and the thalweg could be associated to different roughness-lengths in order to improve the hydrodynamic calibration. This observation is supported by the results of a study on the dunes dynamic on the site [9] which show that the mesoforms adopt different sizes on the thalweg and on the bars. Using several bed roughness on the domain is probably more pertinent.

No relationship seems to link the bed roughness coefficients obtained after the calibration and the water discharge (Table I). This illustrates the complexity of the interactions between hydrodynamic and bed roughness (characterized during floods by complex hysteresis [14]), which depends strongly to the dunes dynamic (in sand-bed rivers as the Loire). The present study highlights this point by showing the influence of the small dunes on the bed roughness and the flows. Indeed, only the dunes longer than 10 m have been integrated in the spatial discretization. It is admitted that the influence of the bedforms smaller than the elements of the meshes is parameterized through the roughness length coefficient [11]. Sensitivity analysis have shown that for a constant k_s, the use of refined meshes and re-interpolated on a more detailed bed topography, gives values of velocities similar to those predicted by calculations with the basic meshes (Fig. 5b). Normally, the bed roughness of the refined meshes should be increased (roughness of the small dunes + *ks* of the models) and the velocities decreased. As it is rarely the case, the results of the sensitive tests indicate that the small dunes seems to not contribute significantly to the bed roughness. Nevertheless, in general, the integration of the small bedforms in the meshes improves the representation of the flow structure. Thus, with the refined and re-interpolated meshes, the distribution of the velocities follow vertical and crosswise variations close to those observed in the field data (Fig. 2e). The integration of the small dunes also improves significantly the calculation of the vertical velocities (Fig. 2f). This indicates that the small bedforms strongly influence the vertical velocities; the latter being linked to the turbulences generated by these small dunes. Thus, if the turbulence affects significantly the sediment dynamics (especially for the suspended sediment and therefore, the von Karman constant), and by extension the morphology of the bed, it seems necessary to integrate the small bedforms into the morphodynamic models. However, it should be noticed that in some cases, the refinement of the mesh modified the bed topography so much that the results of the simulation can be locally degraded.

Calibration and sensitivity tests have showed a systematic overestimation of the velocities predicted for a discharge of 2000 m³/s applied on alternate bars configuration (Fig. 3b and 3d). This can be explained by the not-representation of a secondary channel in the models on the left bank close to the profile P90. Indeed, this secondary channel is totally connected above 1700 m3/s [9]. Thus at 2000 m³/s, the connection of the secondary channel should decrease the water discharge in the main channel (from P90). As the reducing of the water discharge in the models is no considered, the predicted velocities are overestimated compared to the field data. A deeper investigation of the influence of the connection/disconnection of the secondary channel on the main channel's hydrodynamic should improve our understanding of bifurcations.

The results of the models show that the general flow is defined by the channel planform. However, the bars modify the hydrodynamic. Indeed, the macroforms deflect the streamlines and concentrate the flows in the thalweg. Thus, the large flow velocities (Fig. 6) are constrained on the edge of the bars which follow the thalweg. It also seems that the macroforms constitute a physical limit which gives the currents a different structure on either side of the bars. The bars control the location of the divergence and convergence zones, respectively caused by the channel widening and narrowing (Fig. 7). Thus, the separation and the mixing of the currents always take place, respectively, on the crest and downstream of the macroforms. The bars' configurations (i.e. alternate or transverse) in the channel partly determine the location of the large flow velocities and those of the divergence and convergence zones.

This study allowed the validation of TELEMAC-3D to reproduce the hydrodynamics in a complex morphological environment in the presence of transverse and alternate bars. Future work include the coupling to the morphodynamic model (SISYPHE) in order to simulate the sedimentary processes around the bars, for a better understanding of their formation and evolution in natural systems [7].

ACKNOWLEDGEMENT

The measurements were funded by the Master Plan Loire Grandeur Nature-FEDER (Presage n° 30809). The authors thank Philippe Jugé, Yann Guerez, Vincent Bustillo, Benoît Delplancque, Benjamin Gandubert and Olivier Guillemet for their help during the measurements. The four month research scholarship of Benjamin Magnier is gratefully acknowledged.

REFERENCES

[1] M. Colombini, G. Seminara and M. Tubino (1987). "Finite-amplitude alternate bars." Journal of Fluid Mechanics, 181, 1, pp. 213-232.

[2] G. Seminara and M. Tubino (1989). "Alternate bars and meandering: free, forced and mixed interactions." River meandering, S. Ikeda and G. Parker, Washington, American Geophysical Union - Water Resources Monographs 12, p. 267-320.

[3] M. Tubino (1991). "Growth of alternate bars in unsteady flow." Water Resour. Res., 27, 1, pp. 37-52.

[4] S. Lanzoni (2000). "Experiments on bar formation in a straight flume: 1. Uniform sediment." Water Resour. Res., 36, 11, pp. 3337-3349, doi:10.1029/2000WR900160.

[5] M. Tubino, R. Repetto and G. Zolezzi (1999). "Free bars in rivers." Journal of Hydraulic Research, 37, 6, pp. 759-775.

[6] A. Crosato and E. Mosselman (2009). "Simple physics-based predictor for the number of river bars and the transition between

meandering and braiding." Water Resour. Res., 45, 3, pp. W03424, doi:10.1029/2008WR007242.

[7] F. Mattia, D. Wang, J.-M. Hervouet, A. Leopardi, K. El Kadi Abderrezzak and P. Tassi (2013). "Numerical simulations of bar formation and propagation in straight and curved channels." XXth TELEMAC-MASCARET Users conference, Karlsruhe, Germany.

[8] F. C. Wu, Y. C. Shao and Y. C. Chen (2011). "Quantifying the forcing effect of channel width variations on free bars: Morphodynamic modeling based on characteristic dissipative Galerkin scheme." J. Geophys. Res., 116, pp. F03023, doi:10.1029/2010JF001941.

[9] N. Claude (2012). "Processus et flux hydro-sédimentaires en rivière sablo-graveleuse : influence de la largeur de section et des bifurcations en Loire moyenne (France)." PhD, University of Tours, Tours, p. 366.

[10] N. Claude, S. Rodrigues, V. Bustillo, J.-G. Bréhéret, P. Tassi and P. Jugé (2013). "Interactions between flow structure and morphodynamic of migrating bars in a channel expansion/contraction, Loire River, France.", unpublished.

[11] S. D. Sandbach, S. N. Lane, R. J. Hardy, M. L. Amsler, P. J. Ashworth, J. L. Best, A. P. Nicholas, O. Orfeo, D. R. Parsons, A. J. H. Reesink and Szupiany R.N. (2012). "Application of a roughness-length representation to parameterize energy loss in 3-D numerical simulations of large rivers." Water Resour. Res., 48, 12, doi:10.1029/2011WR011284.

[12] J.-M. Hervouet (2007). "Hydrodynamics of free surface flows, modelling with the finite element method", John Wiley & Sons.

[13] E. A. Keller (1971). "Areal sorting of bed-load material: the hypothesis of velocity reversal." Bulletin of the Geological Society of America, 82, 3, pp. 753-756.

[14] R. M. Frings and M. G. Kleinhans (2008). "Complex variations in sediment transport at three large river bifurcations during discharge waves in the river Rhine." Sedimentology, 55, 5, pp. 1145-1171, doi:10.1111/j.1365-3091.2007.00940.x.